Title: | **STRUCTURAL ASSESSMENT OF A CABLE-STAYED BRIDGE**

Author(s): | François M. Hemez, Hoon Sohn

Submitted to:

http://lib-www.lanl.gov/la-pubs/00818603.pdf

STRUCTURAL ASSESSMENT OF A CABLE-STAYED BRIDGE

François M. Hemez[1] and Hoon Sohn[2]
Los Alamos National Laboratory
Engineering Sciences & Applications Division
Weapon Response Group (ESA-WR)
P.O. Box 1663, M/S P946, Los Alamos, New Mexico 87545

ABSTRACT

The structural health monitoring of a large cable-stayed bridge using ambient vibration measurement is summarized. The location of the bridge cannot, at this time, be revealed for confidentiality reason. The bridge is continuously monitored with an instrumentation system that has been collecting 16 channels of acceleration, wind pressure and temperature data over the past six years. The paper focuses on the analysis of two data sets collected in June 1995 and September 2000. Nonlinear data processing techniques such as higher-order statistical and temporal moments and wavelet transforms are presented to quantify the energy content of the signals in the time and frequency domains. Then, linear modal models are fit to the data in order to translate the changes observed in terms of stiffness reduction or damping increase. It is concluded that structural change takes the form of a reduction in stiffness rather than an increase in damping. The discussion also illustrates typical issues encountered in structural health monitoring applications. These include collecting non-stationary signals, investigating a nonlinear response and dealing with environmental variability and changing operating conditions.

NOMENCLATURE

The recommended "Standard Notation for Modal Testing & Analysis" is used throughout this paper [1].

[C]	Matrix of damping coefficients
{F(t)}	Applied forces
[H$_{XF}$]	Transfer function from **{F}** to **{X}**
[K]	Matrix of stiffness coefficients
[M]	Matrix of mass coefficients
p(x)	Probability density function
{q(t)}	Generalized, modal coordinates
[S$_{XF}$]	Power spectral density function
{X(t)}	Physical nodal displacements
$\left\{\hat{X}(s)\right\}$	Fourier transform
[W$_X$]	Wavelet transform
{u$_j$}	jth mass-normalized mode shape
s$_j$	jth radial frequency
d$_j$	jth modal damping ratio
{•}	Vector (N$_R$ rows by 1 column)
[•]	Matrix (N$_R$ rows by N$_C$ columns)
(•)*	Complex conjugate

1. INTRODUCTION

In 1995, a real-time, on-line data acquisition and monitoring system was installed on a large cable-stayed bridge whole location cannot be revealed at this time for confidentiality reason. The purpose of this system is to continuously monitor structural motion, stresses and related environmental and structural data. Bridge operators are remotely alerted if any parameter exceeds specified thresholds, which could indicate a change in the bridge's structural condition and a potential safety concern.

The purpose of this study is to analyze two data sets collected by the monitoring system in June 1995 and September 2000. The central question is to assess whether or not significant changes in the structural condition of the bridge have occurred over these five years. The main premise is that any

significant structural change or deterioration produces changes in the load path or energy dissipation of the bridge, which, in turn, modifies the measured response. Conversely, it is assumed that inferring changes in the system's response is possible and that these changes can be quantified in terms of global structural parameters (strength, stiffness, energy dissipation). The inverse step is a difficult problem especially when the input to the system (wind conditions, traffic loads) and the sources of environmental variability (temperature, humidity, cable tension) are respectively unknown and uncontrollable / unobservable.

2. STRUCTURAL DAMAGE ASSESSMENT

Techniques that have been proposed for Structural Health Monitoring (SHM) can be categorized in two classes, namely, **supervised** learning and **unsupervised** learning [2, 3]. The difference between the two concepts essentially depends on whether data sets are available for **training** (supervised) or not (unsupervised). The training step develops models or relationships between the response of the structure and an indicator of its structural condition.

In this application, the problem is slightly different. Two data sets are available, each for a "known" structural condition. The data collected in June 1995 as the bridge became operational are known to represent the pristine structural condition. The problem is to assess the deviation from this reference of the second data set collected in September 2000 and to translate it in terms of structural information.

More precisely, the main question is to assess whether the change in structural condition takes the form of stiffness reduction or damping increase. Answering this question is important because it could indicate different damage scenarios. Typically, stiffness reduction points to damage in structural elements (loss of stiffness in beams or joints) while an increase in damping points to damage scenarios that involve contact and friction mechanisms. We therefore seek to transform the measured response in the modal space

$$\{\mathbf{X(t)}\} = \sum_{j=1\ldots N_M} \mathbf{q_j(t)}\{\mathbf{u_j}\} \qquad (1)$$

where N_M denotes the order of modal truncation. The well-known linear equation of motion

$$[\mathbf{M}]\{\ddot{\mathbf{X}}(\mathbf{t})\} + [\mathbf{C}]\{\dot{\mathbf{X}}(\mathbf{t})\} + [\mathbf{K}]\{\mathbf{X}(\mathbf{t})\} = \{\mathbf{F}(\mathbf{t})\} \qquad (2)$$

then becomes decoupled into linear, Single Degree-Of-Freedom (SDOF) oscillators

$$\ddot{\mathbf{q}}_{\mathbf{j}}(\mathbf{t}) + 2\mathbf{d}_{\mathbf{j}}\mathbf{s}_{\mathbf{j}}\dot{\mathbf{q}}_{\mathbf{j}}(\mathbf{t}) + \mathbf{s}_{\mathbf{j}}^2\mathbf{q}_{\mathbf{j}}(\mathbf{t}) = \left\{\mathbf{u}_{\mathbf{j}}\right\}^{\mathrm{T}}\left\{\mathbf{F}(\mathbf{t})\right\} \qquad (3)$$

that can be investigated independently of each other. The decoupling of equations shown in equation (3) is achieved because proportional damping is assumed.

Our investigation therefore consists of extracting the modal parameters—frequencies and modal damping ratios—for each data set available. This is performed using the Eigensystem Realization Algorithm (ERA), a subspace identification method that best-fits linear SDOF models (3) to the measured acceleration time history [4]. The frequencies and modal damping ratios extracted from the June 1995 and September 2000 data sets are then compared to assess whether damage takes the form of stiffness reduction or damping augmentation.

It is generally the case with ambient testing that no measurement of the system's input is available. In our case, information about important input parameters such as wind pressure, humidity and traffic loads is not available. Because the input to the system is unknown to a great extent, determining the transfer functions and accounting for environmental variability is impossible. For addressing this difficulty, the commonly accepted approach of replacing the time series by their auto-correlation and cross-correlation functions is adopted. In addition, filtering in the frequency domain is performed to restrict the analysis to specific bandwidths of interest.

Another issue is that the available data sets do not necessarily reflect a linear, stationary and proportionally damped response. To address this problem, time-frequency analysis is performed and several features are extracted to discuss the limitations of our analysis in light of evidence of non-linearity, non-stationarity and non-proportionality.

3. DESCRIPTION OF THE BRIDGE

The bridge investigated is a large cable-stayed bridge. It measures 782 meters (2,566 ft.) in total length including the 450 meters (1,476 ft.) span over a river and two 166 meters (545 ft.) side spans. The bridge's main span is 18 meters (59 ft.) in width. The suspension design is that of a single plane symmetric cable-stayed bridge with 34 cables per pylon. The two supporting pylons are elevated 78 meters (256 ft.) above the deck surface. Finally, it should be mentioned that the deck and two supporting pylons are all manufactured out of structural steel.

     LA-UR-01-5691, Unclassified

The monitoring system used to collect the data sets includes 12 accelerometers, 3 anemometers and one thermocouple. Figure 1 illustrates the location of acceleration sensors on the bridge. In this study, we focus on analyzing the acceleration data collected at only four channels labeled 4, 5, 6 and 8. These four channels are oriented in the vertical direction and they provide the best signal-to-noise ratios. Channels 10, 11, 12 also provide good quality data but their location (on top of the pylon) makes them less relevant for assessing the deck's structural condition. Table 1 summarizes parameters of the data acquisition system for acceleration measurements. Because our investigation is restricted to the global behavior of the bridge, it is believed that the bandwidth of the data acquisition system (0-50 Hertz) is well suited to the frequency band of our interest (0-4 Hertz).

Table 1. Parameters of the data acquisition.

Parameter	Value
Calibration	1.25 Volt/g (+/- 1%)
Sampling rate	200 samples/second
Sensor roll-off frequency	50 Hertz
Anti-aliasing filtering	Digital
Filter cut-off frequency	80 Hertz
Useable bandwidth	0-50 Hertz

Channel	Location
1-V	Side span
2-L	Pylon, deck level
3-T	Pylon, deck level
4-V	½ span, outer
5-V	¼ span, outer
6-V	¼ span, center
7-T	½ span, center
8-V	½ span, center
9-T	¼ span, center
10-L	Pylon top
11-T	Pylon top
12-V	Pylon top

Legend: **L**: Longitudinal,
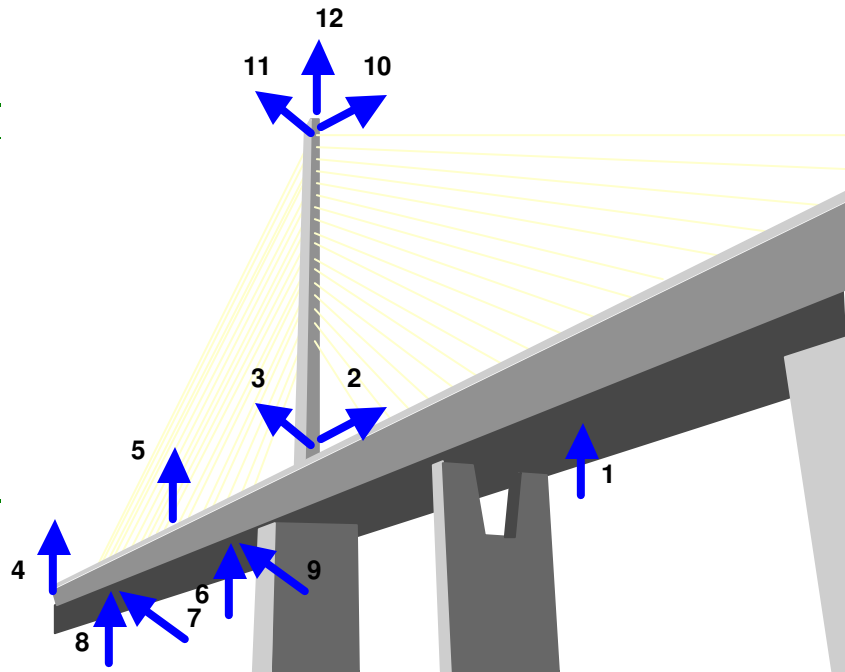**T**: Transverse,
V: Vertical.

Figure 1. Illustration of the bridge and instrumentation system deployed.
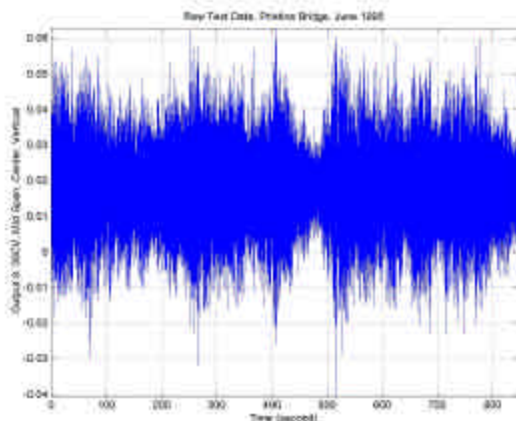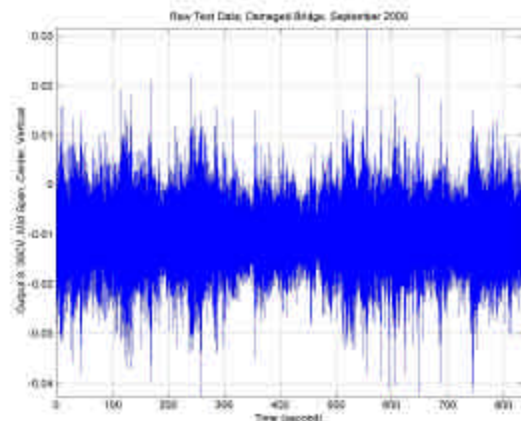
Figure 2. Acceleration at channel 8 (June 1995).

Figure 3. Acceleration at channel 8 (Sept. 2000).

3

Figures 2-3 illustrate typical acceleration signals collected in June 1995 and September 2000. They illustrate that the signal mean values vary from channel to channel and data set to data set. To eliminate any systematic bias, the raw test data are pre-processed by subtracting the mean from each signal.

It can also be observed that values of the acceleration signal at channel 8 in Figure 2 (June 1995) range from –0.04 Volt to 0.06 Volt, approximately, spanning 0.1 Volt of amplitude. Values of the acceleration signal at channel 8 in Figure 3 (September 2000) range from –0.04 Volt to 0.02 Volt, approximately yielding 0.06 Volt of amplitude. The other acceleration signals exhibit similar characteristics. Clearly, the change in structural condition produces a decrease of the acceleration amplitude. Such a trend is counter-intuitive to the generally accepted perception that damage reduces the overall stiffness or increases the flexibility. The reason is that both a reduction in stiffness and augmentation in flexibility would tend to increase the overall motion. Of course, for such a complex structure, one could argue that some damage scenarios, such as the loosening of bolted connections, might have the effect of increasing the dissipation of energy in the system, which could yield less motion.

4. POWER SPECTRUM ANALYSIS

Acceleration responses at channels 4, 5, 6 and 8 are first investigated using the Power Spectral Density (PSD) functions. The PSD transforms time series into a frequency domain. Peaks indicate resonant frequencies and we investigate the effect that potential structural damage might have on the frequency content.

A low-pass 8th-order Butterworth filter is first applied to the time-domain records after the mean of each signal has been removed. The filter's cut-off frequency is set to 4 Hertz to focus our analysis on the first few Hertz of structural response. Then, each filtered signal is split into 30 pseudo-replications of length 5,559 each. The pseudo-replications are averaged to generate a single time-domain record of length 5,559. The final PSD functions $\mathbf{S_{XX}}$ are obtained

$$\hat{\mathbf{S}}_{\mathbf{XX}}(\mathbf{s_k}) = \frac{1}{\mathbf{N_S N_R Dt}} \sum_{i=1...N_R} \left| \hat{\mathbf{X}}^{(i)}(\mathbf{s_k}) \right|^2$$

$$\hat{\mathbf{X}}^{(i)}(\mathbf{s_k}) = \mathbf{Dt} \sum_{l=1...N_S} \mathbf{X}^{(i)}(\mathbf{t_l}) e^{-\frac{2pp j l k}{N_S}}$$

(4)

where **Dt** denotes the sampling interval, **N_S** denotes the number of sampling points, **N_R** denotes the number of averaged pseudo-replicates and $\mathbf{j^2 = -1}$ (see Reference [5] for details). Figures 4-7 compare the PSD curves of channels 4, 5, 6 and 8 in the 0-to-4 Hertz bandwidth. Solid lines indicate the June 1995 responses and dashed lines indicate the September 2000 responses. Overall, it can be observed that similar resonant peaks are present in both data sets. This observation leads to the conclusion that the structural condition has not changed significantly or that the PSD functions at channels 4, 5, 6 and 8 are not sensitive to structural damage (low observability).
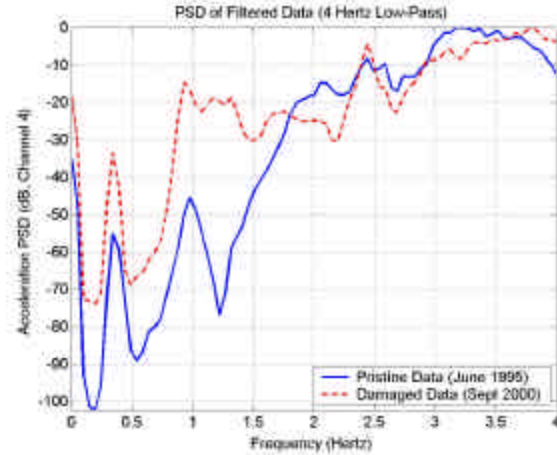

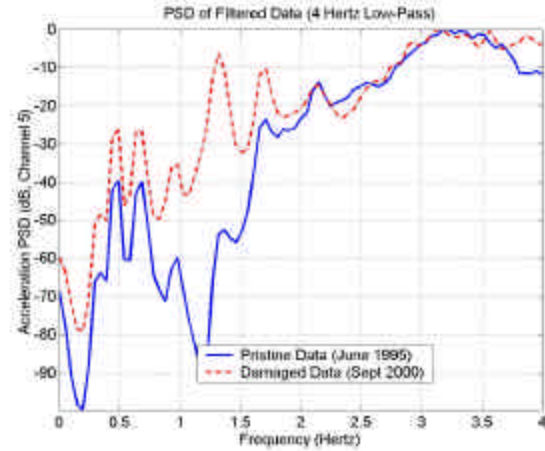**Figure 4. PSD comparison at channel 4.**

Figure 5. PSD comparison at channel 5.

Although the same resonant peaks are visible in both data sets, significant change occurs between 1.0 and 1.5 Hertz. The resonant peak at 1.3 Hertz observed on channels 4, 5 and 6 (and, to a lesser extent, channel 8) in June 1995 disappears in September 2000. This is the most noticeable qualitative change that can be observed from the PSD analysis. We also note that channel 8 indicates more

change than any other channels. This change might have been caused by the fact that the response PSD at channel 8 was not normalized by any kind of input data. Because of its location at the center of the main span, the response collected at channel 8 is expected to be more sensitive to input environments such as traffic loads.
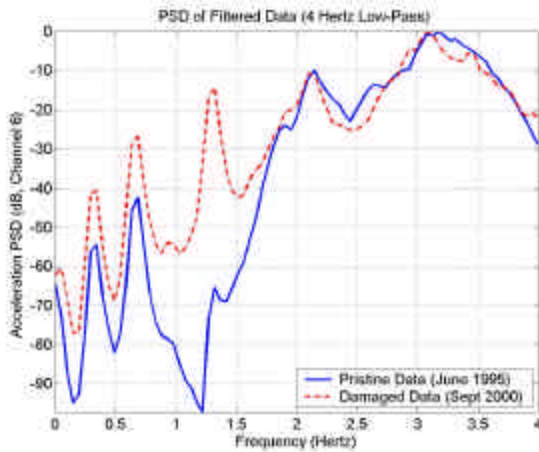

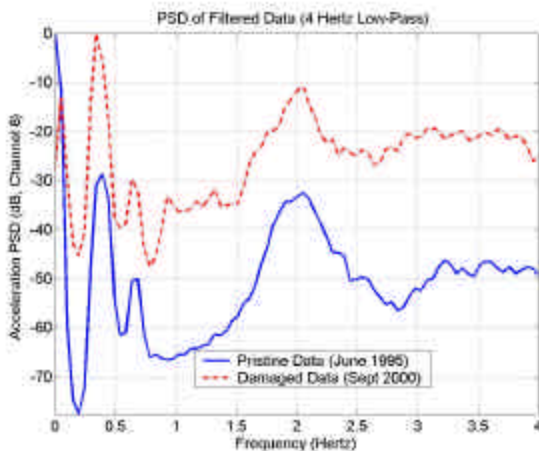**Figure 6. PSD comparison at channel 6.**

Figure 7. PSD comparison at channel 8.

The conclusion of the PSD investigation is that, although the overall agreement between the June 1995 and September 2000 responses is good at channels 4, 5, 6 and 8, significant change in the dynamics occurs around 1.3 Hertz. However, it is difficult to translate such change into stiffness reduction or damping augmentation. Furthermore, no input normalization is performed and it should be kept in mind that the PSD estimation relies on strong assumptions such as the linearity, stationarity and normality (Gaussian signals) of the responses. To examine the validity of these assumptions, other features are investigated next.

5. VERIFICATION OF ASSUMPTIONS

In this section, two non-conventional features are extracted from the data sets and compared. The purpose is to examine the extent to which the linearity and normality assumptions are satisfied and evolve between June 1995 and September 2000. The two features examined are the standard deviation (2nd statistical moment) and kurtosis (4th temporal moment) of the acceleration responses. These features are referred to as "non-conventional" to stress the difference with the ERA-based modal analysis.
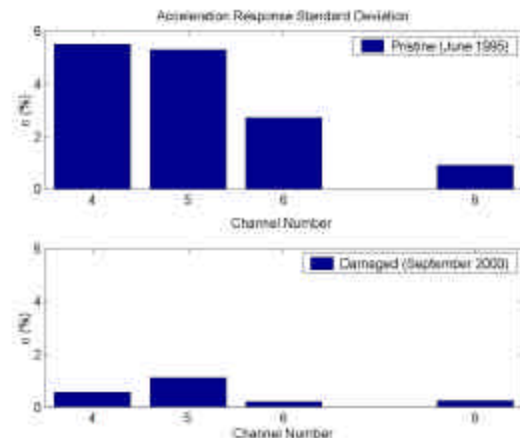

Figure 8. Comparison of signal standard deviations.

Figure 8 compares the signal standard deviation statistics at channels 4, 5, 6 and 8. The most striking difference between the two data sets is the greater response standard deviations exhibited at channels 4, 5 and 6 in June 1995. These levels are about ten times those observed in September 2000. This variation seems unrealistically large but we have no other data sets or measurement records to clarify the cause of this variation. The increased June 1995 standard deviation statistics can also be attributed to a nonlinear or noise-contaminated response. In the remainder, we will therefore exercise caution when using the June 1995 data set as the reference of the pristine structure.

Next, we examine the response Probability Density Function (PDF). The reason is because the PDF, which quantifies the probability that the value of a waveform will be within a given range, is a fundamental characteristic of time series data. Most data analysis techniques assume that the probability density **p(x)** is zero-mean normal (Gaussian), hence, described by

$$p(x) = \frac{1}{\sqrt{2}s} e^{-\left(\frac{x}{\sqrt{2}s}\right)^2} \qquad (5)$$

5

where **x** denotes the signal amplitude and **s** denotes the standard deviation of the data. It is verified that the bridge responses at channels 4, 5, 6 and 8 are roughly Gaussian. Deviation from normality is assessed next.

In general, distributions differ from Gaussian in two main ways. First, a distribution can exhibit more high-amplitude spikes than Gaussian. In this first case, acceleration signals are characteristic of stiffness hardening or rattling behavior. Alternatively, the distribution can exhibit at higher signal magnitudes fewer-than-Gaussian high-amplitude spikes. In this second case, acceleration signals are characteristic of stiffness softening. One measure of the nonlinear properties of the data is the kurtosis, the 4th moment of the time series amplitude distribution [6]. The normalized kurtosis **K** is formally defined from the first four temporal moments **M$_0$**, **M$_1$**, **M$_2$** and **M$_3$** as

$$\mathbf{M_i} = \mathbf{Dt} \sum_{k=1...N_S} (\mathbf{t_k})^i (\mathbf{X(t_k)})^2$$

$$\mathbf{K^3} = \frac{\mathbf{M_3}}{\mathbf{M_0}} + \left(\frac{\mathbf{M_1}}{\mathbf{M_0}}\right)^2 \left(2\frac{\mathbf{M_1}}{\mathbf{M_0}} - 3\frac{\mathbf{M_2}}{\mathbf{M_1}}\right)$$

(6)

The normalized kurtosis is zero for a Gaussian distribution. An excess of peaks gives a positive kurtosis and a deficit of peaks gives a negative kurtosis. Figure 9 illustrates the kurtosis **K** for the June 1995 and September 2000 data sets as a function of channel measurements. Excessive peaks are present especially in the September 2000 data. These could correspond to rattling associated with a gap opening and closing.
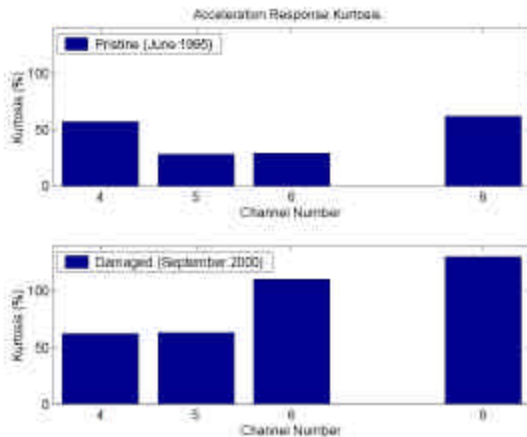

Figure 9. Comparison of signal kurtosis.

Conclusions of this investigation are as follows. First, the large standard deviation statistics observed with the June 1995 data could be the manifestation of

noise contamination. Similarly, the clear increase in the normalized kurtosis could be the result of a nonlinear damage scenario such as the opening and closing of gaps at the locations where sections of the bridge are bolted together. It is most critical to determine what is structural response and what is noise. If the increased standard deviation represents primarily noise, then the first step would be to filter out this noise and to focus on the analysis of the real structural response. This issue is addressed by investigating the degree to which the response is nonlinear (section 6) and focusing the analysis on structural modes (section 7).

6. DATA WAVELET ANALYSIS

In this section, we investigate the degree of non-linearity of the data. This is achieved by using a time-frequency wavelet transform. Wavelets are employed for their ability to filter out noisy components of a signal. Non-linearity and non-stationarity are also investigated.

Wavelets are mathematical functions that decompose a signal into scaled coefficients using a set of wavelet basis functions. The family of basis functions used for wavelet analysis is created by both dilations (scaling **a**) and translations in time (shift **b**) of a "mother wavelet," thereby, providing both time and frequency information about the signal being analyzed. Here, the Morlet wavelet is employed. The wavelet **w$_X$(a,b)** is obtained by convolving the signal **X(t)** with the translations and dilations of the mother wavelet, **W(t)**

$$\hat{\mathbf{W}}_\mathbf{X}(\mathbf{a,b}) = \mathbf{Dt} \sum_{k=1...N_S} \mathbf{W}^*(\frac{\mathbf{t_k - b}}{\mathbf{a}}) \mathbf{X(t_k)}$$

(7)

$$\mathbf{W(t)} = \mathbf{e}^{-(t^2 + 2ppjt)}$$

The Morlet wavelet is a complex valued transform that captures both the magnitude and phase characteristics of a signal while also retaining its temporal nature. Figure 10 shows the wavelet analysis of the data collected in June 1995 at channel 4.

The June 1995 wavelet transform of channel 4 indicates significant resonant dynamics below 10 Hertz. Figure 10 also indicates a series of closely spaced resonant modes that appear consistently throughout the 800-second time record. Such horizontal lines at fixed frequencies tend to indicate stationarity. The same trends are observed at channels 5, 6 and 8. With the data collected in September 2000, the energy content is spread in the 0-to-30 Hertz bandwidth. Because the wavelet transform can filter out noise components from the

signals, energy spreading is attributed to nonlinear interaction between the resonant modes rather than noise contamination.
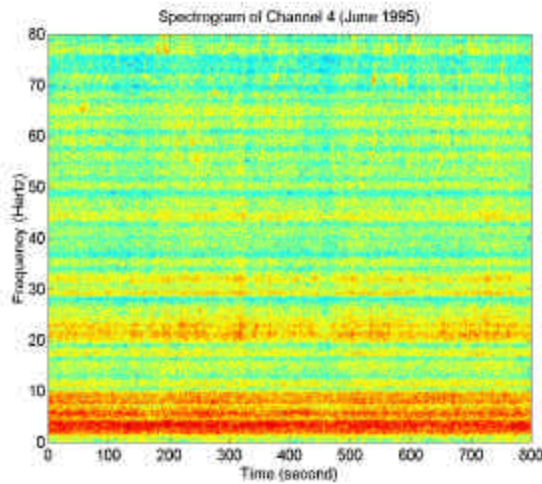

Figure 10. Wavelet of channel 4 (June 1995).

Next, wavelets are used to form transmissibility functions that retain the variability of the system in time. Examination of changes that are occurring at higher frequencies is a good indication of the amount of non-linearity present in the system. By using the Morlet wavelet instead of the Fourier transform, a time-based transmissibility can be formed. The transmissibility between an input **F(t)** and output **X(t)** is defined as

$$\mathbf{H}_{XF}(\mathbf{a},\mathbf{b}) = \frac{\hat{\mathbf{S}}_{XF}(\mathbf{a},\mathbf{b})}{\hat{\mathbf{S}}_{FF}(\mathbf{a},\mathbf{b})} \quad (8)$$

The main difference with a conventional frequency response function is that the auto-correlation and cross-correlation functions in equation (8) are computed using the wavelet transform (7) instead of the Fourier transform. In addition, the input and output signals, **F(t)** and **X(t)**, are selected from the pool of four channels 4, 5, 6 and 8 because no measurement of the system's real input is available. The degree of correlation between transmissibility functions computed from the June 1995 and September 2000 data sets is assessed using the Modal Assurance Criterion (MAC). The MAC is defined as the correlation coefficient between two vectors that collect the transmissibility functions at all time samples and frequency bins of interest.

The lack of symmetry in Table 2 illustrates the dependency of transmissibility functions on the input and output channels. The near symmetry of the MAC matrix restricted to channels 4, 5 and 6 reinforces our opinion that little change occurs to the load path

between any combination of channels 4, 5 and 6. The largest structural change is identified when channel 8 is used as the output. The source and nature of this structural change can however not be determined.

Table 2. Correlation of wavelet transmissibility.

MAC	Input 4	Input 5	Input 6	Input 8
Output 4	N/A	76.5%	87.1%	15.9%
Output 5	74.5%	N/A	86.8%	44.5%
Output 6	86.0%	86.6%	N/A	35.8%
Output 8	51.4%	56.4%	46.3%	N/A

The analysis of wavelet-based transmissibility functions indicates a large change in the response of the structure at channel 8. This change implies that the structure somehow changed in that vicinity between the two data readings. Furthermore, it can be stated with confidence that there is an increase in non-linearity at or around the location of channel 8.

7. SUBSPACE MODAL ANALYSIS

The final analysis presented in this publication is a modal analysis. Our intent is to answer questions such as "Has the stiffness been reduced?" and "Has the dissipation of energy changed?" by characterizing the system in terms of global modal parameters.

As mentioned earlier, the modal parameter identification algorithm used in this study is ERA [4]. Because the sources of ambient excitation were not measured, the impulse response functions needed to run ERA are replaced by the auto-correlation functions **[R$_{XX}$(kDt)]**. Auto-correlation functions are obtained by taking the inverse discrete Fourier transform of the auto-spectral density functions defined in equation (4). Figure 11 shows the frequencies identified from the acceleration time series collected at channels 4, 5, 6 and 8 as the model order—which is defined as twice the number of resonant modes—is varied from 4 to 40, with increments of 4. Frequencies identified from the June 1995 data are indicated with hollow circle marks and frequencies identified from the September 2000 data are indicated with filled circle marks. A resonant mode is identified with reliability when the frequency converges as the model order increases. Some of the modes identified clearly show this convergence pattern, such as the 1st mode around 0.5 Hertz. Modes that seem to "appear" and "disappear" as the model order is varied are generally regarded as computational or "noise" modes as opposed to structural modes.
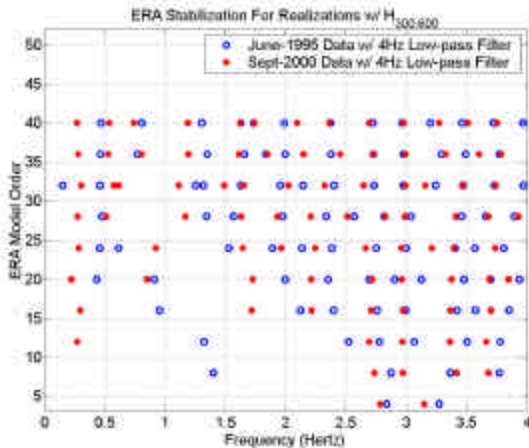
7

Figure 11. ERA/DC stabilization diagram.

From Figure 11, it can be observed that there is a significant frequency shift of the bridge's fundamental mode around 0.5 Hertz. Most of the noticeable change occurs in the 1.0-1.5 Hertz bandwidth. There seems to be a resonant mode around 1.2 Hertz in both data sets but the stabilization diagram shows that this mode is not consistently identified as the model order is varied. These observations agree with the analysis of power spectral density functions discussed in section 4.

We now proceed with the test-to-test correlation. The June 1995 and September 2000 data sets are identified with ERA parameters kept constant so that the algorithm introduces no artificial bias. Time records at channels 4, 5, 6 and 8 consist of 30 averages of pseudo-replications of length 5,559. A low-pass filter with cut-off frequency at 4.0 Hertz is applied. The ERA/DC (Data Correlation) algorithm is implemented with 300 row-blocks, 600 column-blocks and a model order kept constant and equal to 36 (see Reference [4] for details). Computational or "noise" modes are typically associated with high damping levels. The dynamic behavior of the system investigated—a large civil engineering bridge structure—suggests that resonant modes associated with more than 3% modal damping are suspect, especially at low frequencies. Only modes that exhibit a strong convergence in the stabilization diagram, reasonable damping ratios and that satisfy other criteria such as the EMAC and MPC (see Reference [4]) are retained to segregate structural from computational modes. This leads to the five modes listed in Tables 3-4.

Table 3. Test-to-test frequency correlation.

Mode	June 1995	Sept. 2000	Shift
1	0.43 Hertz	0.22 Hertz	-48.8%
2	1.99 Hertz	1.73 Hertz	-13.1%
3	2.90 Hertz	2.72 Hertz	-6.2%
4	3.48 Hertz	2.96 Hertz	-14.9%
5	3.70 Hertz	3.38 Hertz	-8.6%

Table 4. Test-to-test damping correlation.

Mode	June 1995	Sept. 2000	Shift
1	7.6%	2.1%	-72.4%
2	0.8%	1.3%	62.5%
3	1.6%	2.4%	50.0%
4	0.2%	2.1%	950.0%
5	0.3%	1.3%	333.3%

The frequency and damping shifts are listed in percentages of the June 1995 values in Tables 3 and 4, respectively. A negative shift indicates a decrease compared to the June 1995 value. The five modes retained for the analysis witness a consistent decrease in frequency. In terms of modal damping, large increases are observed, sometimes over one order of magnitude (see modes 4 and 5). Such large shifts are observed with caution because ERA is known to be less reliable to identify damping ratios than it is to identify resonant frequencies. It should also be kept in mind that the modal-based fit assumes a proportional viscous damping model. Local non-linearity, such as complex friction mechanisms or the opening and closing of gaps, might produce the effect of coupling some of the resonant modes through the modal damping matrix. In this case, a proportional damping model would not be appropriate. This may explain some of the unrealistic modal damping ratios obtained. It is concluded that the change in structural condition can definitely be cast in terms of stiffness reduction. Damping may have increased but another investigation would be required to confirm this result.

8. CONCLUSION

This publication summarizes an investigation of the structural condition of a large cable-stayed bridge. Difficulties include the unknown sources of ambient vibration and the small number of measurement channels available. The analysis of two data sets collected five years apart suggests a significant decrease of the overall stiffness of the bridge.

However, this assessment is based on fitting linear modal representations to the data sets and comparing global modal parameters. An analysis employing nonlinear data processing techniques— higher-order statistical and temporal moments, wavelet transforms—indicates that the acceleration time series exhibit significant non-linearity, especially in the second data set believed to represent a "damaged" state of the system. This discussion illustrates that the validity of linear modal

representations can be questioned when investigating complex damage scenarios.

REFERENCES

[1] Lieven, N.A.J., Ewins, D.J., "A Proposal for Standard Notation and Terminology in Modal Analysis," *10th International Modal Analysis Conference,* San Diego, CA, Feb. 2-5, 1992, pp. 1414-1419.

[2] Farrar, C.R., Doebling, S.W., Nix, D.A., "Vibration Based Structural Damage Identification," *Philosophical Transactions of the Royal Society: Mathematical, Physical & Engineering Sciences*, Vol. 359, No. 1778, 2001, pp. 131-149.

[3] Sohn, H., Farrar, C.R., "Damage Diagnosis Using Time Series Analysis of Vibration Signals," *Journal of Smart Materials and Structures*, Vol. 10, 2001, pp. 446-451.

[4] Juang, J-N., **Applied System Identification**, 1st Edition, Prentice Hall, London, 1993.

[5] Bendat, J.S., Piersol, A.G., **Random Data: Analysis and Measurement Procedures**, 2nd Edition, John Wiley and Sons, Inc., New York, NY, 1986.

[6] Smallwood, D.O., "Characterization and Simulation of Transient Vibrations Using Band Limited Temporal Moments," *Journal of Shock and Vibration*, Vol. 1, No. 6, 1994, pp. 507-527.

LA-UR-01-5691, Unclassified